Structure and Corrosion Resistance of Vacuum-Arc Multi-period CrN/Cu Coatings

Hanna Postelnyk[1]([✉]) [iD], Oleg Sobol[1] [iD], Ondrej Chocholaty[2] [iD], and Sergey Knyazev[1] [iD]

[1] National Technical University "Kharkiv Polytechnic Institute", 2, Kyrpychova St., Kharkiv 61002, Ukraine
`annapostelnik@ukr.net`
[2] University of West Bohemia, 2732/8, Univerzitní St., 301 00 Pilsen, Czech Republic

Abstract. The influence of deposition conditions (pressure, bias potential, layer thickness) on the structure and corrosion resistance of vacuum-arc multi-period CrN/Cu coatings is studied. For research, we used the methods of precision XRD, scanning electron microscopy with energy dispersive microanalysis, impedance spectroscopy, and potentiodynamic polarization tests to detect corrosion resistance in a solution of 0.9% NaCl. According to structural studies, phases with an fcc crystal lattice are formed in the layers: Cu and CrN mononitride. In CrN layers obtained at the highest bias potential of –200 V, a change in the lattice period associated with the action of compression stresses was revealed. Tests for corrosion resistance showed that for all the samples studied, the corrosion process has a predominantly anodic reaction. The most corrosion-resistant coatings are those obtained at a pressure of $5 \cdot 10^{-4}$ Torr and the greatest bias potential of -200 V in constant rotation mode. The feature of such coatings is the smallest thickness of copper and CrN layers (about 8 nm), the presence of compression stresses (which enhances adhesion between the layers), and the absence of a pronounced texture (the paths of easy diffusion are minimized).

Keywords: Composite coatings · Bias potential · Phase composition · Corrosion rate · Polarization curves · Electrochemical impedance spectroscopy

1 Introduction

The introduction of many modern progressive technologies requires the creation of new materials and the improvement of the properties of already known ones. The task of creating materials with desired properties can be solved through the use of structural engineering [1]. The structural engineering method has shown particularly high efficiency in predicting the properties of materials, the formation of which occurs under highly nonequilibrium conditions. Due to this, it became possible to achieve a wide range of phase, structural, and stress-strain states that cannot be achieved under equilibrium conditions. Such materials include coatings obtained by the vacuum-arc method [2, 3]. In the vacuum-arc method, nitrides are the most technologically

advanced, which provides good wear resistance and corrosion resistance [4, 5]. As a result of this, it was possible to create vacuum-arc multi-period coatings based on transition metal nitrides with very high physical and mechanical properties. In such nanocomposites, chromium nitride has a good prospect for use as a relatively inexpensive and effective material for protection against electrochemical corrosion. In addition, CrN exhibits high-temperature stability and has a relatively low coefficient of friction [5, 6].

2   Literature Review

Austenitic steels are widely used for the manufacture of technical and medical instruments, implants, screws for various purposes, etc. [7, 8]. However, this steel class has low wear resistance and does not have high corrosion resistance (e.g., low resistance to pitting corrosion). It is known that the main cause of corrosion and fatigue wear is the presence of chloride ions in the technological and biological environment [9]. One of the effective ways to extend the service life of such materials is to apply protective coatings that increase the corrosion resistance and wear resistance [10, 11]. The use of the vacuum-arc method allows one to obtain materials that can work under conditions of high temperatures, pressures, and also under the action of aggressive media [12, 13].

A feature of nitride coatings is that they are biocidal [14], i.e. leading to the death of bacteria on their surface. Therefore, nitride coatings can be used for medical instruments, accessories, etc. [15, 16]. In addition, nitrides have a relatively high wear resistance, which significantly exceeds the wear resistance of steels, and nitrides of transition metals are usually more stable in an aggressive environment than many marks of steel. Chromium nitride has good mechanical and corrosive properties and is used as a protective coating at elevated temperatures [17, 18]. A disadvantage of chromium nitride coatings is their relatively high fragility. To increase the plastic properties of chromium nitride coatings, multi-period composites with plastic layers of transition group metals can be used as a component.

Copper has high ductility and practically does not interact with nitrides, and therefore is a very promising material for increasing the ductility of multilayer composites.

Therefore, this work is aimed at studying the effect of technological conditions for the production of multi-period CrN/Cu coatings on their structural-phase state and electrochemical characteristics of corrosion in physiological saline using open-circuit potential, impedance spectroscopy, and potentiodynamic polarization.

3   Research Methodology

Coating substrates were made of AISI 321 austenitic steel. The coatings on the substrate were deposition by the vacuum-arc method at the "Bulat-6" installation with various technological parameters of deposition (Table 1). The working gas pressure (P_N) during deposition of coatings varied within $4 \cdot 10^{-3} \div 5 \cdot 10^{-4}$ Torr; the bias

potential supplied to the substrate was −65 or −200 V. The choice of such regimes was due to the need to verify the influence on the structure and properties of the ion bombardment factor during deposition. The greatest influence of ion bombardment was provided by the $U_b = -200$ V mode at $P_N = 5 \cdot 10^{-4}$ Torr. In this case, the continuous mode (with a constant rotation speed of the substrate during the deposition process) provided the largest specific volume of the mixed material at the interface between the layers. The $U_b = -65$ V, $P_N = 4 \cdot 10^{-3}$ Torr mode is standard for applying CrN coatings with less influence of the ion bombardment factor. In this mode, due to different deposition times, the thickness of the layers changed. This was necessary to change the specific volume of the mixed layer at the boundary (such a volume decreases with increasing layer thickness). Therefore, the deposition was carried out from two sources (Cr and Cu) in the regimes with constant rotation speed (rotation speed of 8 rpm) and in discrete mode (with a stop for 20 s near each of the plasma sources).

Table 1. Technological parameters of deposition.

Series	P_N, Torr	U_b, V	The condition for obtaining
1	$5 \cdot 10^{-4}$	−200	Constant rotation
2	$4 \cdot 10^{-3}$	−65	Constant rotation
3	$4 \cdot 10^{-3}$	−65	20 s interval, 180 layers

The deposition was carried out from two sources (Cr and Cu) in the regimes with constant rotation speed (rotation speed of 8 rpm) and in discrete mode (with a stop for 20 s near each of the plasma sources).

The phase-structural state of the samples was studied by X-ray diffractometry using a DRON-4 apparatus (Cu-K$_\alpha$ radiation). For monochromatization of the detected radiation, a graphite monochromator installed in the secondary beam (in front of the detector) was used [19]. The tables of the Powder Diffraction File international center were used to decode the diffraction patterns. The separation of profiles into components was carried out using the "NewProfile" software package. The surface morphology of the coated samples was investigated using scanning electron microscopy (SEM) (Philips XL30 ESEM).

Coatings were examined for their corrosion resistance during electrochemical processes. Electrochemical tests were carried out using a 3-electrode cell with a capacity of 200 ml and a Biologic SP-150 potentiostat. The cell consists of a coated sample (working electrode), a saturated calomel electrode (reference electrode), and a platinum electrode (counter electrode). Corrosion resistance was assessed by measuring the open-circuit potential for 1.5 h in a solution of 0.9% NaCl at room temperature.

Impedance spectroscopy was performed in the frequency range from 10^{-2} to 10^5 Hz. The potentiodynamic polarization test was carried out in the range from −0.60 to +1 V at a scan speed of 1 mV/s. The contact area of the sample with the electrolyte was 0.196 cm^2.

4   Results

The classical research scheme of modern materials science suggests the following sequence: composition (elemental and phase) - structure (substructure) - properties. Therefore, the first step was the study of elemental and phase compositions. Figure 1 shows the energy dispersive spectra (the top elemental composition calculated from them is shown on the right) of series 1 and 3 before the corrosion test.
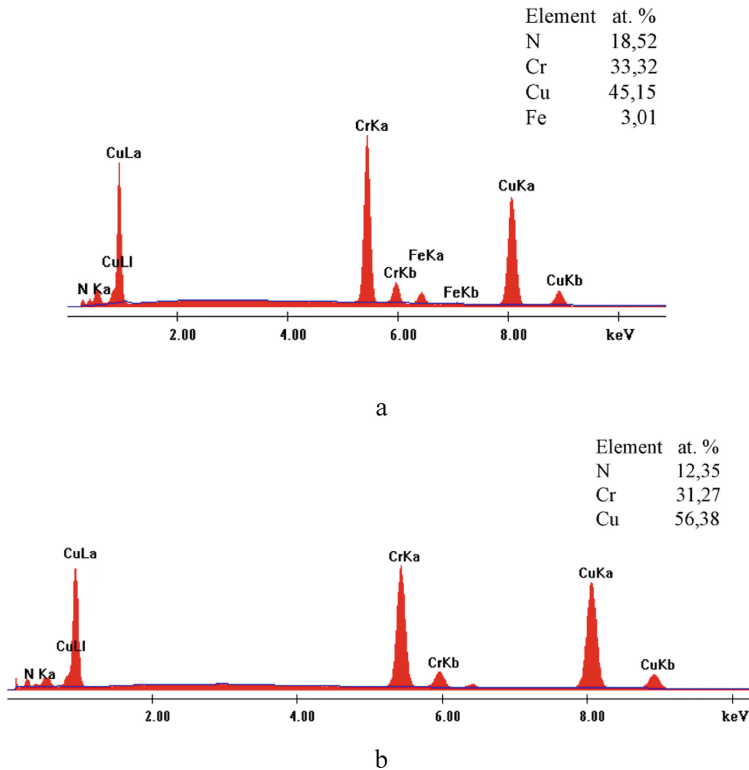

Element	at. %
N	18,52
Cr	33,32
Cu	45,15
Fe	3,01

a

Element	at. %
N	12,35
Cr	31,27
Cu	56,38

b

Fig. 1. Energy dispersive spectra with data on the elemental composition of series 1 (a) and 3 (b) before corrosion tests.

It can be seen that for series 3 obtained in the discrete mode, the relative copper content is much larger. Since, according to the experimental conditions, individual layers of copper were deposited, a large content indicates a greater thickness of the Cu layer.

To study the phase-structural state, the XRD method was used. The X-ray diffraction spectra of the coatings are shown in Fig. 2.

The spectra in Fig. 2 show that the positions of the diffraction peaks correspond well to the fcc lattices of the two phases CrN (JCPDS 76-2494) and Cu (JCPDS 89-2838). The relatively high intensity of the (111) CrN peak for samples of the 2nd series

(spectrum 2 in Fig. 2) indicates the presence in the CrN layers of a predominant orientation with the [111] axis perpendicular to the growth plane. For coatings of the 1st and 3rd series, large peaks are characteristic of the peaks from the (200) plane. The lattice periods calculated from the position of the peaks remain practically unchanged for the Cu layers and amount to a_{Cu} = 3,595 A.
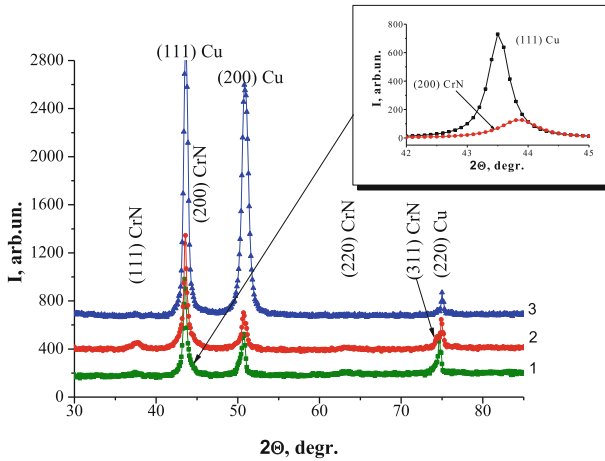

Fig. 2. Plots of diffraction spectra and decomposition of a complex diffraction profile of series 1 into components (insert in the upper right corner). (1 − P_N = 5·10^{-4} Torr, U_b = −200 V (continuous operation); 2 − P_N = 4·10^{-3} Torr, U_b = −65 V (continuous mode); 3 − P_N = 4·10^{-3} Torr, U_b = −65 V (discrete mode, 20 s)

For thinner CrN layers, period changes are observed. The smallest value is a_{Cu} = 4.1402 A (for a sample from the 2nd series), and for samples of series 1 and 3, the period is somewhat longer and is a_{CrN} = 4.1568 (1 series) and a_{CrN} = 4.1541 A (3 series). The most likely reason for this change is the formation of compression stress in the CrN layers.

As a result of the corrosion tests, the potential (E_{corr}) and current (I_{corr}) of corrosion were established (which were calculated using the Tafel extrapolation method). Potentiodynamic polarization curves are shown in Fig. 3.

As can be seen from Fig. 3 - the process is controlled mainly by the anode part of the polarization curves [20]. From the above curves, the slope coefficients of the rectilinear portion of the anodic and cathodic parts β_a and β_c are obtained.

Since the anodic reaction takes precedence for the corrosion process on coatings (the substrate is more electronegative than coatings), the rate of continuous corrosion and not the porosity of the protective coating can be taken into account, for example in [21].

The corrosion rate is proportional to the current of corrosion and was calculated by the formula

$$CR = \frac{I_{corr} \cdot K \cdot EW}{d \cdot A},$$ (1)

where CR is the corrosion rate, mm/year; I_{corr} - corrosion current, mA; K is the conversion factor determining the unit of measurement of the corrosion rate; EW - equivalent weight, gram-equivalent; d is the density, g/cm^3; A is the sample area, cm^2.
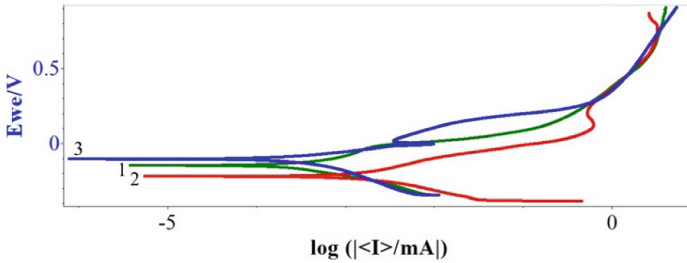

Fig. 3. Potentiodynamic polarization curves.

The calculation results are given in Table 2.

Table 2. Potentiodynamic polarization test results.

Series	E_{corr}, mV	I_{corr}, mA	β_a, mV	β_c, mV	CR mm/year
1	−99,241	$2{,}08 \cdot 10^{-4}$	68,3	149,8	$9{,}78 \cdot 10^{-3}$
2	−200,829	$8{,}72 \cdot 10^{-4}$	95,1	106,1	$41 \cdot 10^{-3}$
3	−229,129	$1{,}69 \cdot 10^{-3}$	550,4	218,3	$79{,}6 \cdot 10^{-3}$

Samples with a minimum corrosion current have the lowest corrosion rate. The best indicators of corrosion resistance are provided by coating samples obtained at a relatively low nitrogen pressure. Such coatings are practically not textured (Fig. 2) and therefore have few easy diffusion paths (due to a large number of misoriented intergranular boundaries). Moreover, the use of the constant rotation mode of the substrate has a clear advantage over the discrete deposition mode (due to the formation of thinner (nanometer) layers). Therefore, high corrosion resistance is most likely ensured by low diffusion mobility and rapid formation of an oxide film under conditions of oxygen deficiency during testing.

For a better understanding of the kinetics of the process, a graph of the potential change versus time is constructed and analyzed (Fig. 4).
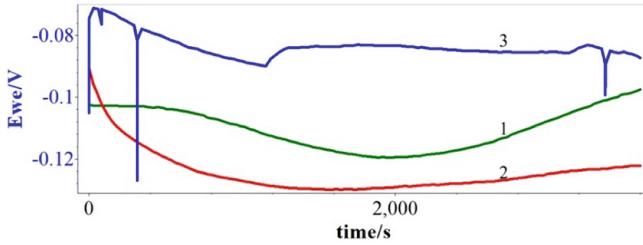
Fig. 4. Curves of the corrosion potential over time.

As can be seen from the curves in Fig. 4 for series 3, a sharp dissolution of the coating (first minute of testing) followed by passivation is characteristic. The presence of peaks and a change like a curve may indicate damage to the passivating layer and the protective coating as a whole. To verify this assumption, the surface morphology of the samples was studied after corrosion tests (Fig. 5).
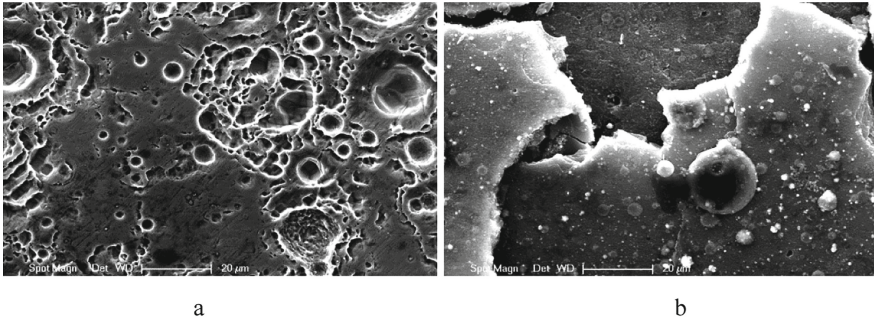

a   b

Fig. 5. Surface morphology of series 1 (a) and 3 (b) after corrosion tests in 0.9% NaCl.

From Fig. 5b (series 3), total surface destruction is seen, which is consistent with the course of curve 3 in Fig. 4. Energy dispersive analysis (Fig. 1b), performed before corrosion tests, showed an increased copper content, which indicates a different thickness of the layers in the coating under a discrete deposition mode. As a result, during the corrosion process, copper was dissolved in the electrolyte (after corrosion tests, the amount of copper decreased to 6.66 at.%, While the number of other elements increased: N – 39.96 at.%, Cr – 52.14 at.%) causing damage to the coating.

Samples obtained in other modes (Fig. 4, curves 1, 2) tend to passivation and superpassivation, which is associated with an increase in the valence of chromium (Cr^{3+}) with the implementation of reactions:

$$Cr(OH)_3 + 5OH^- - 3e \rightarrow CrO_4^{2-} + 4H_2O \tag{2}$$

$$2Cr^{3+} + 7H_2O - 6e \rightarrow Cr_2O_7^{2-} + 14H^+. \tag{3}$$
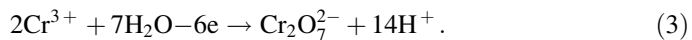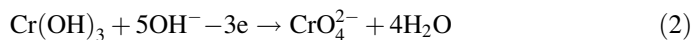
A study of the surface of such coatings, such as series 1, after corrosion tests (Fig. 5a), confirms the absence of destruction, only the formation of "pits" with a developed surface relief is observed (the elemental composition of the coating remains almost unchanged).

As can be seen from a comparison of the curves of changes in potential, coating morphology, phase-structural state, and elemental composition, the resistance of coatings is ensured by the technological conditions for their production, mainly, by the continuous rotation of the substrate, which determines a small layer thickness of about 8 nm.

To obtain additional data on the corrosion resistance of the coatings, the polarization resistance was calculated using the formula

$$R_p = \frac{\beta_a \cdot \beta_c}{2,303 \cdot I_{corr} \cdot (\beta_a \cdot \beta_c)}. \tag{4}$$

The charge transfer resistance was also evaluated through protective coatings using Nyquist curves. The curves themselves for the systems under consideration are shown in Fig. 6. Comparing the diameters of the loops on the Nyquist graph, we can evaluate the corrosion properties of the samples: loops of larger diameter correspond to greater corrosion resistance.
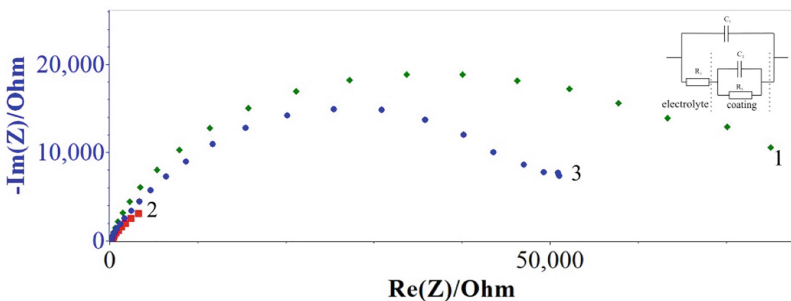

Fig. 6. Nyquist curves and equivalent circuit model "electrolyte-coating". (C_1, C_2 – the capacity of the double layer and coating, respectively; R_1, R_2 – resistance of the electrolyte and phases in the coating, respectively)

This simulated equivalent circuit (Fig. 6) is in good agreement with the experimental values.

Corrosion processes associated with stray currents, charge accumulation and charge transfer through the electrolyte-coating interface can provide clarifying data necessary for understanding the corrosion resistance under real conditions. The data from calculations by formula (2) R_p (polarization resistance) and graphical calculations of the Nyquist curves (Fig. 6) R_{ct} (charge transfer resistance) are presented in Table 3.

Table 3. Corrosion resistance indicators according to the results of calculations of the Tafel curves and graphical analysis of Nyquist curves.

Series	I_{corr}, mA	R_p, Ohm·cm^2	R_{ct}, Ohm·cm^2
1	$2{,}08 \cdot 10^{-4}$	19208	14677
2	$8{,}72 \cdot 10^{-4}$	4900	3274
3	$1{,}69 \cdot 10^{-3}$	7840	10515

5   Conclusions

Studies have shown that the composite multi-period CrN/Cu coatings obtained under different application conditions in the environment of the formation of chloride ions, for the protective mechanism, are anode. Technological formations of coatings with high corrosion resistance were determined: reduced nitrogen pressure ($5 \cdot 10^{-4}$ Torr), high bias potential (−200 V) and deposition mode, which leads to the smallest layer thickness (about 8 nm). With these parameters, a structure is formed without a pronounced predominant orientation, and a large bias potential of −200 V allows the mixing process to go through at the interlayer boundary and leads to the formation of compressive stresses. When using the lower bias potential of U_b during the deposition process, the corrosion resistance of the coatings decreases significantly, and the corrosion rate increases by more than 4 times. The reason for this may be significantly less mixing at the interface between the layers (and, accordingly, a decrease in adhesive bond). With an increase in the thickness of the layers, at which the specific contribution of the mixed layer to the total thickness decreases, the corrosion rate increases even 2 times.

The assessment showed that with a coating thickness of about 10 μ, its work resource in the environment of the formation of chloride ions is about a year.

With a greater thickness of the copper layers (added as a stress relaxer in the microvolumes of the coating), destruction of the coating occurs due to the intense dissolution of the copper layers.

References

1. Sobol', O.V., Andreev, A.A., Gorban', V.F., Stolbovoy, V.A., Meylekhov, A.A., Postelnyk, A.A.: Possibilities of structural engineering in multilayer vacuum-arc ZrN/CrN coatings by varying the nanolayer thickness and application of a bias potential. Tech. Phys. **61**(7), 1060–1063 (2016)
2. Öztürk, A., Ezirmik, K.V., Kazmanlı, K., Ürgen, M., Eryılmazb, O.L., Erdemirb, A.: Comparative tribological behaviors of TiN, CrN and MoNCu nanocomposite coatings. Tribol. Int. **41**(1), 49–59 (2008)
3. Polychronopoulou, K., Rebholz, C., Demas, N.G., Polycarpou, A.A., Gibson, P.N.: Effect of Cu content on the tribological performance of Cr-N coatings at high temperatures (840°C). In: ASME/STLE 2009 International Joint Tribology Conference, pp. 115–117 (2009)

4. Conde, A., Navas, C., Cristóbal, A.B., Housden, J., de Damborenea, J.: Characterisation of corrosion and wear behaviour of nanoscaled e-beam PVD CrN coatings. Surf. Coat. Technol. **201**(6), 2690–2695 (2006)

5. Dinu, M., Mouele, S.M., Parau, A.C., Vladescu, A., Petrik, L.F., Braic, M.: Enhancement of the corrosion resistance of 304 stainless steel by Cr–N and Cr(N, O) coatings. Coatings **8** (132), 1–20 (2018)

6. Martinez, E., Romero, J., Lousa, A., Esteve, J.: Wear behavior of nanometric CrN/Cr multilayers. Surf. Coat. Technol. **163–164**, 571–577 (2003)

7. Wang, Q., Zhou, F., Wang, C., Yuen, M.F., Wang, M., Qian, T., Matsumoto, M., Yan, J.: Comparison of tribological and electrochemical properties of TiN, CrN, TiAlN and a-C: H coatings in simulated body fluid. Mater. Chem. Phys. **158**, 74–81 (2015)

8. Hsu, C.H., Huang, C.K., Ou, K.L.: Improvement on hardness and corrosion resistance of ferritic stainless steel via PVD-(Ti, Cr)N coating. Surf. Coat. Technol. **231**, 380–384 (2013)

9. Sun, Y., Rana, V.: Tribocorrosion behaviour of AISI 304 stainless steel in 0.5 M NaCl solution. Mater. Chem. Phys. **129**, 138–147 (2011)

10. Kim, Y.J., Byun, T.J., Lee, H.Y., Han, J.G.: Effect of bilayer period on CrN/Cu nanoscale multilayer thin films. Surf. Coat. Technol. **202**, 5508–5511 (2008)

11. Niu, Y., Wei, J., Yu, Z.: Microstructure and tribological behavior of multilayered CrN coating by arc ion plating. Surf. Coat. Technol. **275**, 332–340 (2015)

12. Sobol, O.V., Andreev, A.A., Gorban, V.F., Meylekhov, A.A., Postelnyk, A.A., Stolbovoy, V.A.: Structural engineering of the vacuum arc ZrN/CrN multilayer coatings. J. Nano Electron. Phys. **10**, 06030-1–06030-5 (2018)

13. Sobol', O.V., Postelnyk, A.A., Meylekhov, A.A., Andreev, A.A., Stolbovoy, V.A., Gorban, V.F.: Structural engineering of the multilayer vacuum arc nitride coatings based on Ti, Cr, Mo and Zr. J. Nano Electron. Phys. **9**(3), 03003-1–03003-6 (2017)

14. Osés, J., García Fuentes, G., Fernández Palacio, J., Esparza, J., Antonio García, J., Rodríguez, R.: Antibacterial functionalization of PVD coatings on ceramics. Coatings **8**(5), 197–208 (2018)

15. Schmitz, T.: Functional coatings by physical vapor deposition (PVD) for biomedical applications. Würzburg (2016)

16. Kuppusami, P., Elangovan, T., Murugesan, S., Thirumurugesan, R., Khan, S., George, R.P., Ramaseshan, R., Divakar, R., Mohandas, E., Mangalaraj, D.: Microstructural, nanomechanical and antibacterial properties of magnetron sputtered nanocomposite thin films of CrN/Cu. Surf. Eng. **28**, 134–140 (2012)

17. Martinez, E., Sanjines, R., Karimi, A., Esteve, J., Levy, F.: Mechanical properties of nanocomposite and multilayered Cr–Si–N sputtered thin films. Surf. Coat. Technol. **180–181**, 570–574 (2004)

18. Benkahoul, M., Robin, P., Martinu, L., Klemberg-Sapieha, J.E.: Tribological properties of duplex Cr–Si–N coatings on SS410 steel. Surf. Coat. Technol. **203**, 934–940 (2009)

19. Sobol', O.V., Shovkoplyas, O.A.: On advantages of X-ray schemes with orthogonal diffraction vectors for studying the structural state of ion-plasma coatings. Tech. Phys. Lett. **39**(6), 536–539 (2013)

20. Ramoul, C., Beliardouh, N.E., Bahi, R., Nouveau, C., Abdelghani, D., Walock, A.: Surface performances of PVD ZrN coatings in biological environments. Tribol. Mater. Surf. Interfaces **13**, 12–19 (2018)

21. Montesano, L., Gelfi, M., Pola, A., Colombi, P., La Vecchia, G.M.: Corrosion resistance of CrN PVD coatings: comparison among different deposition techniques La. Metallurgia Italiana **2**, 3–11 (2013)